Beyond thermodynamic defect models: A kinetic simulation of arsenic activation in CdTe

D. Krasikov and I. Sankin

First Solar Inc., Perrysburg, Ohio 43551, USA

To overcome the limitations of thermodynamic defect models, we introduce a multilevel kinetic approach to simulate the activation of p doping in CdTe by group V elements using arsenic as a "model" dopant. On the lowest level, we calculate thermodynamic and kinetic parameters of point defects, complexes, and reactions from first principles. On the intermediate level, we use these parameters to calculate the kinetic rates of defect reactions. Finally, we simulate the time evolution of defects and free carriers. Our results show the importance of kinetic factors in defect chemistry models. We reveal the primary arsenic activation pathway to be a fast reaction in which the tellurium atoms get kicked out and replaced on the regular anion sites by interstitial arsenic species. We discover the important role of $(As_i As_{Te})$ and $(As_i As_i)$ complexes that arise during activation anneal to form kinetically stabilized transient states that not only compensate the doping but also can produce deep recombination levels. We expect that our modeling approach and the gained insight into the atomic processes behind the doping formation will advance the defect chemistry modeling of electronic properties of materials.

I. INTRODUCTION

Relatively low absorber doping is the most commonly acknowledged challenge in thin-film CdTe photovoltaics (PV) that prevents this technology from reducing the gap between achieved and theoretical limits of performance. Despite the decades of development, Cu-based processes were not able to produce stable p-type doping in CdTe absorbers above $10^{15} \, cm^{-3}$. On the other hand, several group V elements, namely arsenic, phosphorus, and antimony, have been shown to form p-type doping of $> 10^{16} \, cm^{-3}$ both in single- and polycrystalline CdTe [1–3], making group V elements an appealing alternative to copper for the next generations of CdTe PV.

Recent experimental studies suggest that the activation efficiency of arsenic or phosphorus (the ratio of uncompensated ionized acceptor concentration to the atomic concentration of dopants) can reach 50% in single-crystal CdTe (sx-CdTe) [3,4], while in polycrystalline CdTe (px-CdTe) films it is always lower and reaches 10% at most [2]. Both in sx-CdTe and in px-CdTe, the activation efficiency of group V dopants decreases with the increased incorporation [1,3,5], and can be improved by creating Cd overpressure [2–4]. It can be further improved by reducing the amount of oxygen during CdTe deposition and arsenic activation anneal steps [6,7]. Here, we define "activation anneal" as a thermal process applied to activate previously incorporated dopant. An apparent correlation between the measured time-resolved photoluminescence lifetime and the activation efficiency of phosphorus and arsenic is another experimental observation related to the subject [3,8–10].

Although demonstrated in principle, the highest efficiency devices reported [11] at 22% are doped with copper and not with a more preferable group V dopant. Integration of group V dopant incorporation and activation into an established process flow optimized for decades presents a formidable challenge for commercialization. Further, it is unclear whether incomplete activation leads to other performance-limiting mechanisms, such as increased recombination due to the generation of new point defects in the device. Therefore, a detailed theoretical insight into the process of group V doping activation is required for practical implementation of group V doping into CdTe-based solar cells.

Currently, most theoretical works that analyze the dopants' activation efficiency employ a thermodynamic approach assuming a complete equilibration of all defect reactions [12,13]. Such an assumption is not justified by default, especially in case of relatively low-temperature processing steps. The energy barriers in the way of defects diffusion and reactions introduce kinetic limitations that slow down defect reactions so that complete equilibration cannot be achieved in the limited time of the process step. Hence, the assessment of kinetic limitations is required to justify the usage of the thermodynamic equilibrium approach. An alternative and more general approach is to employ kinetic defect chemistry models that, in addition to thermodynamic properties of defects, utilize their kinetic properties. Such models that naturally support kinetic limitations can be used in simulation of competing mechanisms and analyses of the transient states absent in thermodynamic analysis.

The goal of this study is to investigate defect chemistry of group V acceptor activation on the level of zero-dimensional time- and temperature-bound kinetic simulations. To reduce the complexity of the discussion, we use arsenic as a model dopant that qualitatively represents behaviors of group V elements in CdTe and related alloys. Our simulations take into account the kinetics of defect transformations during activation anneal omitted in the previous study of arsenics activation [13]. Unlike the previous studies, we include all possible pair-defect complexes that may form during activation anneal and supplement the activation reactions with competing compensation reactions. Besides relatively

well-understood defect species such as As_i, As_{Te}, and AX center (distorted As_{Te} defect with As–Te bond formed), this work studies the properties of other point defects and complexes including kinetically stabilized transient states that affect the activation efficiency of arsenic dopant. We also study the dependence of arsenic activation on its atomic concentration and temperature, and discuss the effect of cooldown after high-temperature treatment. Finally, we make high-level assessment of possible impact of arsenic doping on bulk recombination.

The paper is organized in the following sections:

(i) Section II describes simulation methodology starting from atomistic modeling up to kinetic defect chemistry models;

(ii) Section III discusses arsenic activation process in CdTe, which includes description of the properties and behaviors of the point defect and complexes as well as kinetic mechanisms involved in their formation. This section also presents the results of comprehensive kinetic simulations.

(iii) Section IV discusses the scope and limitations of the model and approach employed in this work;

(iv) Section V provides the summary and conclusion of this study.

II. METHODOLOGY

A. First-principles calculations

We perform first-principles calculations using the *ab initio* total-energy and molecular-dynamics package VASP (Vienna *Ab initio* Simulation Package) developed at the Institut für Materialphysik of the Universität Wien [14] and integrated into MEDEA® software environment [15]. Most of the calculations we perform using computational resources of Ohio Supercomputer Center (Columbus, OH).

To find the most favorable atomistic configuration of point defects and complexes in each charge state, we optimize the 216-atom supercell containing the defect by minimizing the forces on each atom below 0.02 eV/Å. There, we use conjugated gradient method, Perdew-Burke-Ernzerhof generalized gradient approximation (GGA-PBEsol) density functional [16], plane-wave basis set with 400-eV cutoff energy, and projector augmented wave (PAW) [17,18] technique that describes interactions between the core states and valence electrons.

After optimization, we calculate the total energy of a supercell using HSE06 hybrid functional [19] based on PBEsol density functional. In this work, we present only the results obtained for the experimental lattice constant of 6.48 Å and PBEsol functional that reproduces the experimental lattice constant with great accuracy (see Sec. III A for details). Using the above techniques, we find the most stable atomic configurations of defects by selecting those with the lowest HSE06 energy. For the interstitial defects species, we analyze all possible interstitial positions in CdTe zinc-blende structure (*Ta* and *Tc* sites with tetrahedral surrounding [20], *M* site with hexagonal surrounding [21,22], anion split or *A* split [23], cation split or *C* split [24], line-type anion interstitial or *A* line [25]). For complexes with interstitial defects, we analyze

all the possible structures based on the properties of isolated interstitial defects.

After selecting the minimum energy pathway (MEP) for the defect diffusion and transformation, we locate the transition state on MEP and calculate the transition-energy barrier with respect to the initial state using climbing image nudged elastic bands method followed by dimer optimization of a transition state and HSE06 calculation of the total energy.

B. Kinetic simulations of defect chemistry

Let us consider a chemical reaction that occurs in semiconductor crystal and operates on species R and P that could be regular lattice sites, free carriers, point defects, or complexes [26]:

$$\sum R_i \underset{R_B}{\overset{R_F}{\rightleftarrows}} \sum P_j. \tag{1}$$
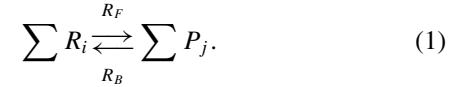
In the forward ("left-to-right") direction, reaction (1) generates the products P while consuming reactants R and the backward reaction produces reactants while consuming products. The forward and backward reaction rates are proportional to the concentrations $[R_i]$ and $[P_j]$ of reactants and products, respectively [27]:

$$R_F = K_F \prod [R_i]$$
$$R_B = K_B \prod [P_j]. \tag{2}$$

Although the proportionality coefficients K_F and K_B in Eq. (2) are commonly referred to as reaction-rate *constants*, their values may depend on environmental factors (e.g., temperature) that define kinetic properties of species. Typically, it is convenient to estimate just one of rate constants from kinetic considerations, and express the other one through the equilibrium reaction constant $K_{EQ} = K_F/K_B$, which does not depend on kinetic properties of species.

To derive K_{EQ}, let us consider the equilibrium state of reaction (1) that requires zero-reaction Gibbs energy, meaning that cumulative chemical potential of products must be equal to that of reactants [27]:

$$\Delta_r G = \sum_{i=1}^{N} \mu_{R,i} - \sum_{j=1}^{M} \mu_{P,j} = 0. \tag{3}$$

Condition (3) can be rewritten in more detail by expressing chemical potentials via energies of formation of involved species and their configurational entropies in approximation of diluted concentrations [28]:

$$\Delta_r G = \sum \left[H_f^{R,i} + kT \ln \left(\frac{N_{EQ}^{R,i}}{N_S^{R,i}} \right) \right]$$
$$- \sum \left[H_f^{P,j} + kT \ln \left(\frac{N_{EQ}^{P,j}}{N_S^{P,j}} \right) \right] = 0. \tag{4}$$

In Eq. (4), sets of parameters (H_f^R, N_{EQ}^R, N_S^R) and (H_f^P, N_{EQ}^P, N_S^P) represent the energy of formation, equilibrium concentration, and density of states for the reactants and products, correspondingly. In this work, we obtain the formation energies of the neutral defect species $H_f^{(0)}$ and

their thermodynamic ionization levels from first principles similarly to previous works [29,30]. We neglect the contributions of volume relaxation to defect formation energies and reaction energies because these contributions are small ($\ll$0.1 eV) [31]. We also do not include the vibrational entropy contributions to the formation energies because of their significant computational cost. These contributions may become noticeable at high temperatures; however, they usually remain in 0.1–0.2-eV range even at 900–1000 K [32,33] and would not change conclusions of our work. Given $H_f^{(0)}$ and thermodynamic ionization levels $\varepsilon_{(i-1)/i}^{VB}$ of the charged defect in $\pm n$th ionization state with respect to the valence-band maximum E_V, we calculate its energy of formation as $H_f^{(n\pm)} = H_f^{(0)} \mp \sum_{i=1}^{n} [\varepsilon_{(i-1)/i}^{VB} + E_V]$. We note that in our approach, the interactions of defects with free electrons and holes are described by detailed reactions similarly to Kröger's approach [26] rather than by a term in defect formation energy used in the grand canonical approach [31]. This allows us to capture the effect of free carriers on defect reactions not only under equilibrium conditions, but also in steady state and in any transient regime.

The density of states represents another fundamental characteristic of a species. In the case of free carriers (electrons and holes), their densities of states equal the conduction- and valence-band densities of states, respectively. When describing a non-free-carrier defect species, we find the density of states N_S as the lattice site density in the host material n_0 multiplied by the atomic and electronic degeneracy factors, g_{atom} and g_{elect}, correspondingly:

$$N_S = g_{atom} \cdot g_{elec} \cdot n_0. \qquad (5)$$

We define electronic degeneracy similarly to Ma *et al.* [33]. For the atomic degeneracy, we use the number of different equivalent atomic positions that a defect or complex can occupy in the unit cell of the host material. In CdTe, this number equals to the index of a symmetry subgroup (from 1 to 24) to which defect or complex belongs. The highest-symmetry defects (full tetrahedral symmetry, *Td*) have the lowest atomic degeneracy 1 and, hence, the lowest density of states, while the lowest symmetry, *C*1, have the highest degeneracy of 24.

By introducing standard reaction Gibbs energy $\Delta_r G^{\Theta} = \sum H_f^{P,j} - \sum H_f^{R,i}$, expression (4) could be further rearranged in the form of mass action law as

$$\prod \frac{N_S^{R,i}}{N_{EQ}^{R,i}} = \prod \frac{N_S^{P,j}}{N_{EQ}^{P,j}} \exp\left[-\frac{\Delta_r G^{\Theta}}{kT}\right]. \qquad (6)$$

In equilibrium, the forward and backward reaction rates are equal, meaning that $K_F \prod N_{EQ}^{R,i} \equiv K_B \prod N_{EQ}^{P,j}$. Therefore, expression (6) could be used to derive thermodynamic equilibrium constant as

$$K_{EQ} = \frac{K_F}{K_B} = \frac{\prod N_S^{P,j}}{\prod N_S^{R,i}} \exp\left(-\frac{\Delta_r G^{\Theta}}{kT}\right). \qquad (7)$$

The mass action law [Eq. (7)] provides the foundation for our analysis. It enforces thermodynamic consistency of the rate constants and it allows us to select the rate constant (K_F or K_B) to approximate from kinetic considerations to obtain better accuracy. Since a reaction can go both ways, the

nomenclature (i.e., which direction to consider as "forward" as opposite to "backward" and which subset of involved species to consider as "reactants" as opposite to "products") becomes a matter of convenience. Upon calculating one of the rate constants from kinetic considerations, the other one follows directly from Eq. (7).

Depending on the approach used to approximate the forward rate constant, we arrange reactions in such a way that forward reactions fall into two main categories: diffusion limited and barrier limited.

Diffusion-limited reaction is a bimolecular reaction that involves two spatially separated reactants, meaning that at least one of them should be mobile for the reaction to occur. After the defects find each other in space, they react to form a product (point defect or complex). If the second step, i.e., the reaction between adjacent defects, happens much faster than the initial diffusion process, one can assume that the reaction event occurs once the reactants come within certain "capture" distance (this approximation is sometimes referred to as "black-sphere" approximation [34,35]). Provided the capture radius R_C and diffusivities of the reactants, the rate constant of such a reaction is given by

$$K_F = 4\pi(D_1 + D_2)R_C, \text{ where } \sum D_i > 0. \qquad (8)$$

For the diffusivities D in Eq. (8), we use a standard expression where we calculate diffusion barriers E_D and prefactors D_0 according to the multiple-barrier diffusion theory [36]:

$$D = D_0 \exp\left(-\frac{E_D}{kT}\right). \qquad (9)$$

Reactions most commonly attributed to this category include those between reactants without electrostatic repulsion. If at least one of the reactants is neutral, we approximate the capture radius as a half-width of the unit cell. If the reactants experience electrostatic attraction, we estimate the capture radius as the "escape" or Onsager radius, the distance between the charges when Coulombic energy is equal to thermal energy kT [37]. Given integer numbers θ_1 and θ_2 of elementary charges carried by the reactants and the dielectric constant of the host material, one can find this distance as

$$R_C = q^2 \frac{|\theta_1 \theta_2|}{4\pi \varepsilon \varepsilon_0 kT}, \quad \theta_1 \theta_2 < 0. \qquad (10)$$

In the case of diffusion-limited reaction of a defect capturing a free carrier, one can neglect the defect's diffusivity and simplify the expression for the rate constant using notation of capture cross section σ_C and thermal velocity of the free carrier v_{th}:

$$K_F = v_{th}\sigma_C. \qquad (11)$$

Although *ab initio* methods to calculate capture cross sections were developed in recent years, in this study we use fixed values of $\sigma = 10^{-15}/10^{-16}$ cm^2 for the capture on neutral/repulsive defects.

Barrier-limited reaction is a monomolecular reaction that transforms a single reactant into one or two products by overcoming an energy barrier. In the case where a reaction results in two products, we assume product separation fast enough to not influence the reaction rates. Note that when it is

not the case, e.g., when the products experience electrostatic attraction, it might be more convenient to consider the backward reaction as forward, and analyze it as diffusion limited. The rate constant of a barrier-limited monomolecular reaction depends on the frequency of attempts ν to jump across the energy barrier E_B as

$$K_F = \nu \cdot \exp\left(-\frac{E_B}{kT}\right). \qquad (12)$$

Although the frequency of elementary atomic jumps ν may exhibit certain temperature dependence, in this study we assume it constant and equal to 5 THz.

In any chemical reaction (1), the production rate of a particular species depends both on the forward and backward components as shown in Eq. (2). For example, a species R_i is produced by the backward reaction and consumed in the forward, so that its net production rate is $R_{R,i}^{net} = R_B - R_F$. Similarly, the net production rate of a species P_j in this reaction is $R_{P,j}^{net} = R_F - R_B$. Moreover, a species may participate in multiple reactions simultaneously; therefore, its overall net production rate becomes a sum of its net production rates in individual reactions [27]. Since the reaction rate is the number of individual transformations that occur in unit volume per unit time, we can model evolution of concentrations of N distinct species involved in M chemical reactions by solving a system of N ordinary differential equations (ODEs):

$$\frac{dU_n}{dt} = \sum R_{n,m}^{net}, \quad n = 1 : N, \quad m = 1 : M. \qquad (13)$$

In Eq. (13), U_n is the concentration of the nth species, and $R_{n,m}^{net}$ is the net production rate of this species in the mth reaction. We solve the system of ODEs implicitly in time domain.

III. RESULTS AND DISCUSSION

This section discusses the arsenic activation process in CdTe. This includes description of the properties and behaviors of the point defect and complexes as well as kinetic mechanisms involved in their formation. Here, we also present the results of comprehensive kinetic simulations.

A. Point defects and complexes formed by As and Te

1. Interstitial arsenic defect As_i

Interstitial arsenic defect As_i is a mobile defect species that has a diffusion barrier of $\leqslant 1.07$ eV (Table I) and this facilitates arsenic diffusion in CdTe crystal. This defect can occupy different charge states depending on the Fermi-level position [Fig. 1(a)]. Similarly to Cl_i defect, it can act as a donor when the Fermi level is low and also can act as an acceptor at high Fermi-level values [12,38]. Moreover, similarly to Cl_i, it tends to occupy different types of lattice sites in different charge states. In thermodynamic equilibrium, the most stable charge states are $+3$, $+1$, and -1 (Fig. 2), which have atomic configurations Ta, cation split C_{spl}, and anion split A_{spl}, respectively. Both $+1$ and -1 charge states play important roles in arsenic activation at high temperature as they can form arsenic acceptor As_{Te} either in exchange reaction or by recombination with tellurium vacancy.

TABLE I. Properties of the point defects and complexes used in our simulations.

Point defect or complex	Symmetry	g_{atom}	g_{elect}	Diffusion prefactor, cm^2/s	Diffusion barrier, eV
$As_{i,C_{spl}}^{+}$	C_s	12	2	0.0052	1.07
$As_{i,Ta}^{3+}$	T_d	1	2	0.0070	0.45
$As_{i,A_{spl}}^{-}$	C_s	12	1	0.00078	0.55 [2]
$Te_{i,A_{spl}}^{0}$	C_{2v}	6	1	0.007	0.09 [36]
$Te_{i,C_{spl}}^{2+}$	C_{3v}	4	1	0.007	0.38 [36]
V_{Te}^{0}	C_{2v}	6	1		
V_{Te}^{2+}	T_d	1	1	0.021	1.70
As_{Te}^{-}	T_d	1	1	0.0052	2.7
As_{Te}^{+}/AX	C_s	12	2	0.0052	2.7
$(As_iAs_i)^{2+}$	C_2	12	1	0.0052	2.20
$(As_{Te}As_{i,Ta})^{2+}$	C_{3v}	4	1	0.0017	1.93
$(As_{Te}As_{i,spl})^{0}$	C_{2v}	6	1	0.0017	1.93
$(As_iTe_i)^{+}$	C_1	24	2		
$(Te_iTe_i)^{0}$	C_1	24	1		
$(Te_iTe_i)^{2+}$	C_{3v}	4	1		

2. Substitutional arsenic defect As_{Te} and AX center

Substitutional arsenic defect As_{Te} is a relatively shallow acceptor that plays a major role in the formation of p-type doping. For the $0/-1$ transition, we calculate a value of 0.12 eV. In agreement with Yang *et al.* [13], we find that As_{Te}^{-} can partially convert into AX^{+} donor configuration by trapping two holes and bonding with the neighboring tellurium anion site [Fig. 1(b)]. Since such conversion plays an important role in arsenic autocompensation, we carefully analyze the stability of the AX center. Previous calculations by Yang *et al.* [13] predict that AX^{+} defect is stable at Fermi levels below ~ 0.36 eV. Fermi-Dirac statistics suggests that high AX-center stability obtained by Yang *et al.* prohibits achieving stable densities of holes above 10^{14} cm^{-3} because of strong autocompensation of As_{Te}^{-} by AX^{+} donors. This result contradicts experimental observations of hole densities in excess of 5×10^{16} cm^{-3} measured in CdTe by Hall technique [1]. In order to find the reason for such discrepancy, we compare the stability of AX center calculated with CdTe lattice constants of 6.48 Å (experimental) and 6.58 Å (used by Yang *et al.* [13]). We found that using the PBEsol functional with experimental lattice constant results in less-stable AX^{+} center with $+/-$ ionization level of only 0.12 eV, which may explain high p-type density achieved in experiments. According to our HSE06 calculations, conversion from symmetric As_{Te} into AX requires overcoming 0.49-eV energy barrier. Our kinetic simulations show that although this barrier does not prevent such conversion during high-temperature anneal, high hole densities in CdTe are still achievable due to relatively unstable AX center.

3. Interstitial tellurium defect Te_i

During an activation anneal, interstitial tellurium defect Te_i appears as a product of exchange reaction in which an arsenic
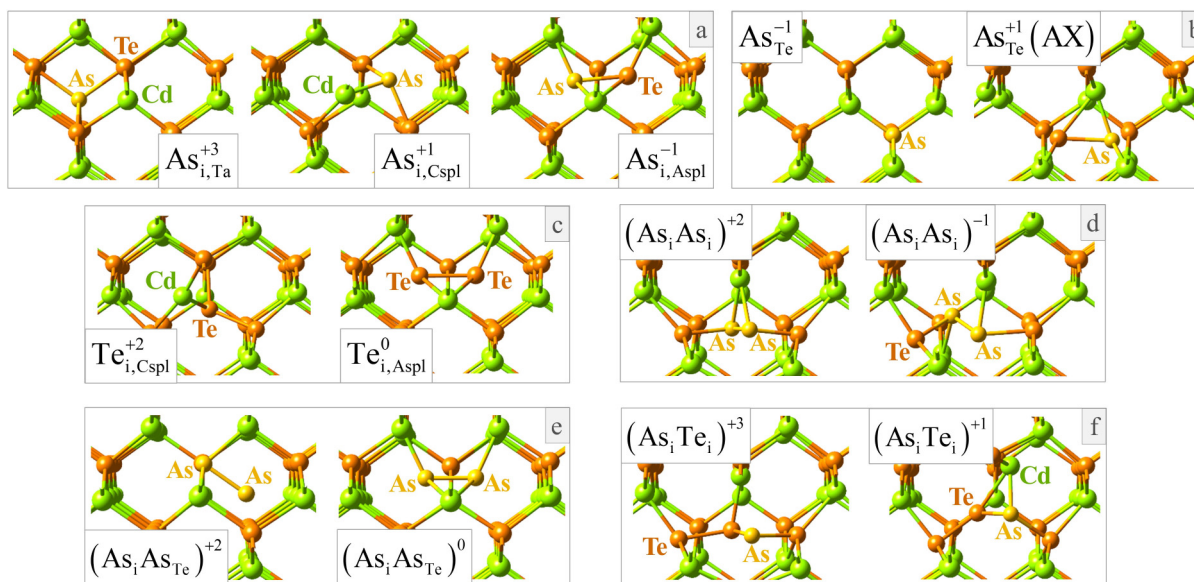
FIG. 1. Atomic structure of the most stable configuration of defects and complexes in different charge states: (a) As_i defect, (b) As_{Te} defect, (c) Te_i defect, (d) (As_iAs_i) complex, (e) (As_iAs_{Te}) complex, (f) (As_iTe_i) complex.

atom replaces tellurium on a regular anion site. Therefore, the properties of Te_i are important for understanding this activation pathway. Our results on atomic structure of Te_i defect agree with Ma *et al.* [24]. According to our calculations, Te_i is a deep double-donor defect with $+2/0$ thermodynamic ionization level at 0.38 eV above the valence-band maximum. In a system with low doping or during high-temperature anneal, Te_i will be mostly neutral, while it tends to convert into $+2$ state in highly p-doped system and/or during cooldown. The activation barriers for Te_i diffusion in 0 and $+2$ charge states are 0.09 and 0.38 eV, respectively [36], which makes it the fastest known point defect in CdTe.

4. Tellurium vacancy defect V_{Te}

Tellurium vacancy defect V_{Te} is a double donor with a $(+2/0)$ ionization level at 0.3 eV from the conduction-band minimum. For structure of V_{Te} defects, our results agree with results by Du *et al.* [23]. Similar to other vacancies, it tends to recombine with available interstitial defects.

5. (As_iAs_i) complex

Association of two As_i^+ defects results in formation of $(As_iAs_i)^{2+}$ double-donor complex [Fig. 1(d)], which is energetically favorable among pair complexes analyzed in this and our previous work [30]. Despite electrostatic repulsion, As_i^+ defects tend to bind into $(As_iAs_i)^{2+}$ complexes and compete with formation of arsenic acceptors. Figure 3 shows the association energy of (As_iAs_i) and in comparison with association energy of $(As_{Te}As_i)$ complex, another important player in arsenic activation mechanism.

6. $(As_{Te}As_i)$ complex

Association of As_i^+ donor and As_{Te}^- acceptor results in formation of $(As_{Te}As_i)$ complex [Fig. 1(e)]. Although less thermodynamically stable than (As_iAs_i), this complex forms in significant concentrations suppressing arsenic activation
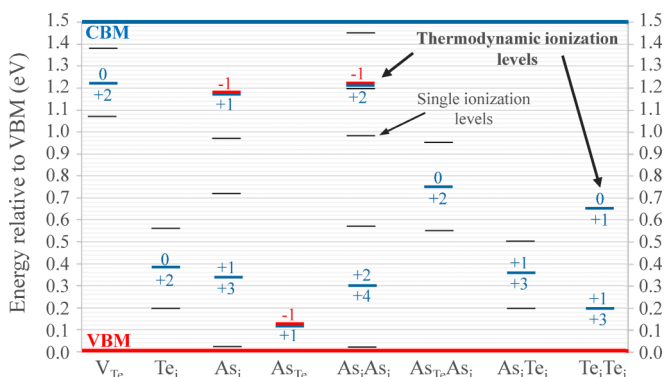

FIG. 2. Ionization levels of defect and complexes. Thick lines with numbers show thermodynamic ionization levels and corresponding charge states; thin lines show single ionization levels for secondary charge states.
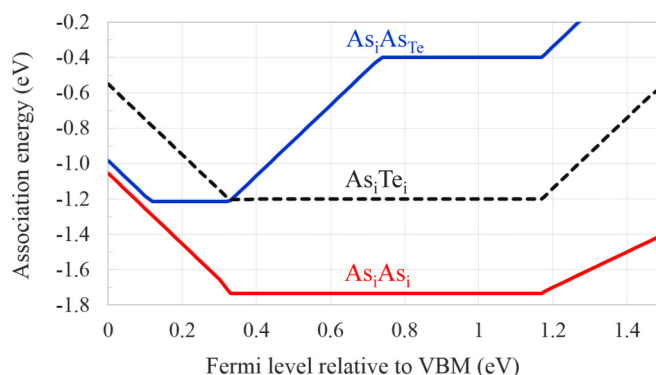

FIG. 3. Association energies of the most important As-related complexes calculated taking into account the most stable states of complexes and separate point defects at a given Fermi level (see Eq. (8) in our previous work [29]). The horizontal lines indicate defect association without the change of charge state; the inclined lines indicate association with the change of charge state.

even at high annealing temperatures. As a double-charged donor in p-type CdTe, this complex plays an important role in arsenic autocompensation.

7. (As$_i$Te$_i$) complex

Association of interstitial arsenic and tellurium defects results in formation of (As$_i$Te$_i$) donor complex. Its primary charge states in CdTe are $+1$ and $+3$, and the $+3$ state is stable in strongly p-type material (Fig. 2).

8. (As$_{Te}$Te$_i$) complex

An intermediate state that forms during activation, complex (As$_{Te}$Te$_i$) may exist in donor and acceptor configurations. In both configurations, an arsenic atom occupies the regular anion site, while a tellurium atom occupies the neighboring M-interstitial site in the donor configuration $(As_{Te}Te_{i,M})^+$, and A-split interstitial position in the acceptor configuration $(As_{Te}Te_{i,spl})^-$.

9. (Te$_i$Te$_i$) complex

(Te$_i$Te$_i$) complex can form when there are enough isolated Te$_i$ defects formed during arsenic activation. The primary charge states of this complex include $+3, +1, 0$.

10. Other defects and complexes

In addition to defects and complexes listed above, only interstitial cadmium defect Cd$_i$ could participate in doping compensation. However, we do not expect it to form in significant concentration ($\sim 10^{18}$ cm^{-3}) during arsenic activation. We do not find any stable defect complexes formed with Cd$_i$.

Table I summarizes the properties of point defect and complexes discussed in this section. These properties include the symmetry, atomic and electronic degeneracy factors, diffusion prefactor, and diffusion barrier. Using this information, we formulate defect reactions and assemble a system of ODEs (13) to study the mechanism of arsenic activation in CdTe.

B. As activation mechanism

To become an activated acceptor in CdTe and related alloys, an arsenic atom has to occupy an anion site in crystalline lattice. Only two reactions ultimately result in the formation of arsenic acceptor defect As$_{Te}$:

$$As_i + V_{Te} \leftrightarrow As_{Te}, \quad (14)$$

$$As_i + Te_{Te} \leftrightarrow As_{Te} + Te_i. \quad (15)$$
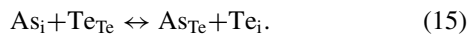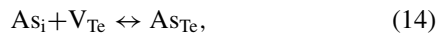
Reaction (14) forms As$_{Te}$ by recombination of interstitial arsenic As$_i$ on anion vacancy V_{Te}, and the exchange reaction (15) forms As$_{Te}$ as the tellurium atom is kicked out and replaced on the anion site by an interstitial arsenic. In this section, we analyze these two options to conclude on the primary activation mechanism and formulate the reduced reaction set that describes arsenic activation.

TABLE II. Reactions included in As activation mechanism via V_{Te}.

Reaction	Standard reaction Gibbs energy, eV
$Te_i^0 + V_{Te}^0 \leftrightarrow Te_{Te}$	-4.83
$As_{i,Cspl}^+ + V_{Te}^0 \leftrightarrow As_{Te}^+$	-2.54
$As_{i,Aspl}^- + V_{Te}^{2+} \leftrightarrow As_{Te}^+$	-4.71

1. Arsenic activation via recombination with tellurium vacancy V_{Te}

This mechanism assumes that tellurium vacancies either preexist in CdTe crystal or form during the activation process. Although previous studies have shown annealing in Cd overpressure at $T > 900$ °C [39] to form tellurium vacancies in CdTe crystal, there are no reports on a method to form required amounts of these defects (e.g., $> 10^{16}$ cm^2) at practical temperatures below 600 °C. Very high formation energy of tellurium Frenkel pair (4.85 eV) and the presence of other impurities competing for the right to recombine with tellurium vacancies make this mechanism of arsenic activation rather impractical. Our kinetic simulation with reactions from Table II shows that even with instant removal of Te$_i$ from the reaction zone, the formation of $\sim 10^{16}$ cm^{-3} of V_{Te} would take more than 10^7 years at 450 °C (Fig. 4).

Formation of V_{Te} on CdTe surface is more favorable and faster than in the bulk, but in this case, diffusion of vacancies becomes a strong limiting factor. We calculate the V_{Te} formation kinetics due to supply from the surface with very high concentration gradient of 10^{18} cm^{-3}/$1\mu m$ and using our calculated V_{Te} diffusion barrier of 1.7 eV, and it takes more than 10^5 s to form 10^{18} cm^{-3} of vacancies (Fig. 4). Based on these assessments, we conclude that arsenic activation via recombination with tellurium vacancy cannot serve as the prime mechanism to achieve strong p-type doping in CdTe absorbers.

2. Arsenic activation via exchange reaction (Te kick-out by As$_i$)

This subsection discusses the second mechanism of arsenic activation in which interstitial arsenic replaces tellurium on
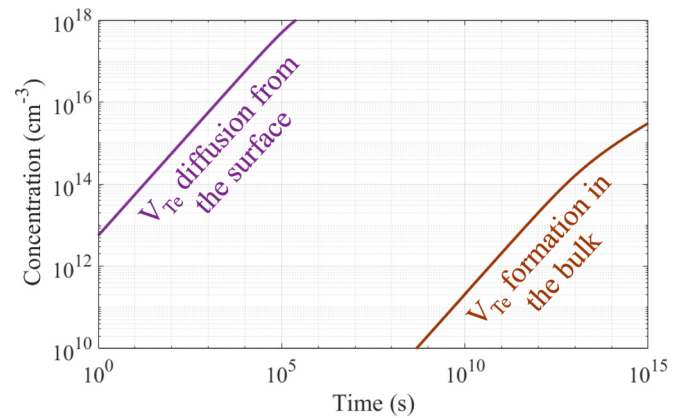

FIG. 4. Kinetics of V_{Te} accumulation at 450 °C by Frenkel pair formation and due to diffusion from the surface. Diffused concentrations shown at 1 μm from the surface.
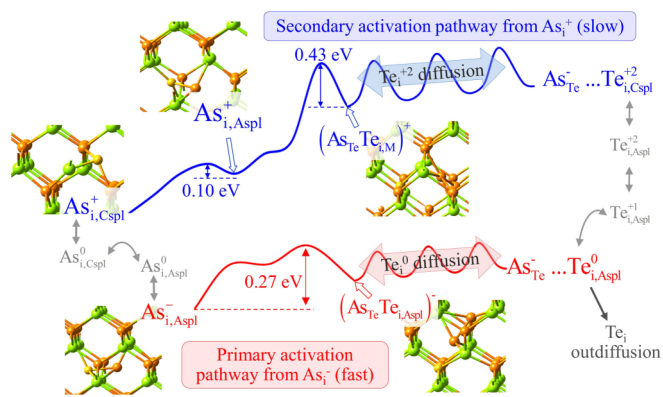
FIG. 5. Detailed schematic of two pathways for Te kick-out by As during As activation process. Primary activation pathway (bottom left to bottom right, marked red) comprises kick-out Te lattice atom by negatively charged As_i^- defect with formation of intermediate short-lived complex $(As_{Te}Te_{i,Aspl})^-$ that quickly dissociates into As_{Te}^- and Te_i^0 defects. Secondary activation pathway (top left to top right, marked blue) comprises kick-out Te lattice atom by positively charged As_i^+ defect with formation of intermediate short-lived complex $(As_{Te}Te_{i,,M})^+$ that quickly dissociates into As_{Te}^- and Te_i^{+2} defects. Also included in schematic are the processes of change of charge state of As_i on the left side and Te_i on the right side (marked gray).

the regular anion site [Eq. (15)]. The properties of MEP determine the kinetics of the activation process and the resulting defect composition after it is completed. Based on careful analysis of possible atomic configurations and their transformations during activation process, we identify two competing activation pathways originating from different charge states of interstitial arsenic, As_i^+ and As_i^-. Figure 5 provides a schematic illustration of these pathways.

The slower activation pathway (upper pathway in Fig. 5) has overall enthalpy cost of $+1.45$ eV upon transition from As_i^+ to "separated As_{Te}^- and Te_i^{2+}" state, which is offset by a configuration entropy gain due to formation of an additional point defect. This pathway consists of a "local" reaction chain $As_{i,Cspl}^+ \leftrightarrow As_{i,Aspl}^+ \leftrightarrow (As_{Te}Te_{i,M})^+$ followed by the fast dissociation of $(As_{Te}Te_{i,M})^+$ complex. Our detailed kinetic simulations suggest that we can neglect intermediate states $As_{i,Aspl}^+$ and $(As_{Te}Te_{i,M})^+$, and instead, describe this pathway by a single diffusion-limited reaction without loss of accuracy:

$$As_{Te}^- + Te_{i,Cspl}^{2+} \leftrightarrow As_{i,Cspl}^+. \qquad (16)$$
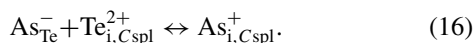
Similarly, we describe the fast pathway (lower pathway in Fig. 5) by a single barrier-limited reaction:

$$As_{i,Aspl}^- \leftrightarrow As_{Te}^- + Te_{i,Aspl}^0. \qquad (17)$$
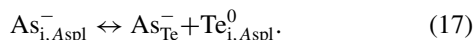
Because of a very small overall reaction energy of 0.12 eV and insignificant reaction barrier of 0.27 eV, we consider this pathway described by reaction (17) as the prime mechanism of arsenic activation in CdTe. Note that both the pathways assume efficient removal of interstitial tellurium by-product from the reaction zone. Since the diffusion barrier for the neutral interstitial tellurium defect in CdTe is below 0.1 eV, the only process limiting its removal would be its segre-

TABLE III. Reactions describing the formation of arsenic acceptor and compensating donor defects.

Reaction	Reaction barrier, eV	Standard reaction Gibbs energy, eV
$As_{i,Aspl}^- \leftrightarrow As_{Te}^- + Te_{i,Aspl}^0$	0.27	0.12
$As_{Te}^- + Te_{i,Cspl}^{2+} \leftrightarrow As_{i,Cspl}^+$		-1.45
$Te_{i,Aspl}^0 \leftrightarrow Te_{segr}$	0.1	-2.00
$As_{i,Cspl}^+ + Te_{i,Aspl}^0 \leftrightarrow (As_iTe_i)^+$		-1.25
$As_{Te}^- + As_{i,Cspl}^+ \leftrightarrow (As_{Te}As_i)^0$		-0.42
$As_{Te}^- + As_{i,Te}^{3+} \leftrightarrow (As_{Te}As_i)^{2+}$		-0.96
$(As_iAs_i)^{2+} \leftrightarrow 2As_{i,Cspl}^+$	3.20	$+1.90$
$As_{Te}^+ \leftrightarrow AX^+$	0.49	0.00

gation or transformation into stable low-energy state. This may include segregation on extended defects or interfaces, formation of secondary phases, and escape into gas state in form of Te_2 molecules. According to the calculated defect formation energies [12], even in Te-rich conditions, the energy of Te_i^0 that escapes to Te bulk is -2 eV, which provides an efficient sink for Te_i^0 by-products. In our simulations, we model the process of Te outdiffusion using a barrier-limited reaction:

$$Te_{i,Aspl}^0 \leftrightarrow Te_{segr}. \qquad (18)$$

C. Competition between As activation and passivation

In addition to As activation reactions described in Sec. III B 2, multiple competing defect reactions can take place, causing incomplete activation while producing compensating defect species. The complete set of activation and competing reactions is summarized in Table III. Using this set of reactions we simulate the arsenic activation anneal for different process temperatures and different initial concentration of As_i^0 defect. These simulations assume instantaneous application of heat and transition from room temperature RT) to process temperature at time zero. Figure 6 shows simulated evolution of concentrations of defects and free carriers during a 30-min anneal at 400 °C starting from initial concentration of $As_i^0 = 10^{18} cm^{-3}$. Based on our results, we can conditionally discriminate three stages of the overall activation-compensation process (black arrows in Fig. 6).

Stage 1: Onset of As_{Te}^- formation. The initial conversion of interstitial arsenic defect into substitutional acceptor happens very fast, within 10^{-7} s. Such fast conversion becomes possible due to very small 0.12-eV enthalpy loss and low reaction barrier of Eq. (17), which comes in a drastic contrast with Cu activation mechanism in CdTe, where kick-out of Cd atom by Cu_i^+ occurs in expense of by about 1-eV enthalpy loss [12,30].

Stage 2: Formation of $(As_iAs_{Te})^{2+}$ and $(As_iAs_i)^{2+}$ compensating donors. Since the activation pathway described by reaction (16) is a relatively slow process due to 1.45-eV energy cost, significant amounts of interstitial arsenic donors As_i^+ remain in the system after completion of stage 1. These species start associating with substitutional arsenic acceptors and with each other forming compensating
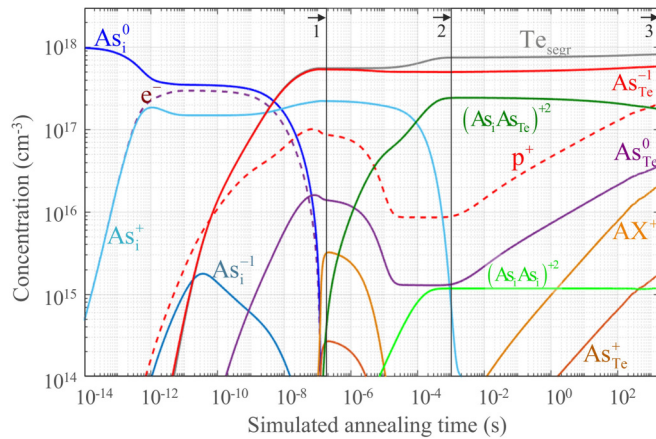
FIG. 6. Simulated temporal evolution of concentrations of defects, complexes (solid), and free carriers (dashed) during 400 °C/30 min activation annealing. Simulation starts from initial concentration $As_i^0 = 10^{18}$ cm^{-3} (left edge) and ends with formation of As_{Te}^-, As_{Te}^0, As_{Te}^+, AX defects, $(As_iAs_{Te})^{2+}$ and $(As_iAs_i)^{2+}$ complexes and excess free hole density (right edge). Three stages of As activation are shown by numbers on top: (1) Onset of As_{Te}^- formation, (2) formation of $(As_iAs_{Te})^{2+}$ and $(As_iAs_i)^{2+}$ compensating donors, and (3) slow increase of activation efficiency.

double-charged donor complexes. Despite lower association enthalpy, $(As_iAs_{Te})^{2+}$ complex accumulates faster comparing to its counterpart $(As_iAs_i)^{2+}$ due to electrostatic attraction between As_i^+ and As_{Te}^- defect species and because of the large amount of As_{Te}^- produced by reaction (17) at stage 1. In addition, a very short-lived concentration buildup of $(As_iTe_i)^+$ donor complexes is possible in this stage. Figure 7 provides a schematic illustration of activation and passivation pathways in stages 1 and 2.

The amount of arsenic donor complexes accumulated in stage 2 depends on the total concentration of arsenic atoms
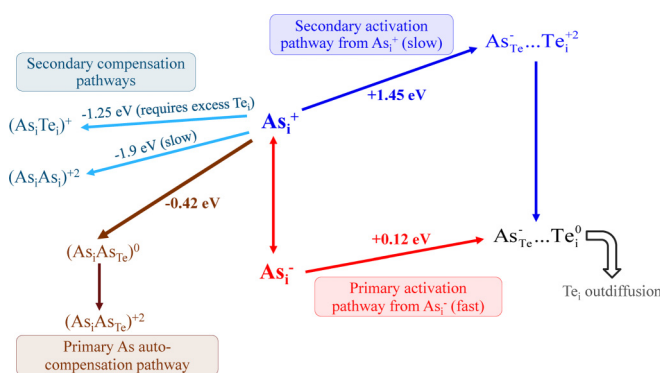

FIG. 7. Schematic of primary As activation and compensation pathways corresponding to defect reactions in Table III. Right part of schematic shows primary and secondary As activation pathways starting from As_i^- and As_i^+, respectively. Left part of schematic shows primary and secondary compensation pathways with formation $(As_iAs_{Te})^{2+}$ and $(As_iAs_i)^{2+}$ complexes, respectively. During activation anneal, interstitial As partially activates into As_{Te}^- state (center to right) and partially converts into compensating complexes (center to left).
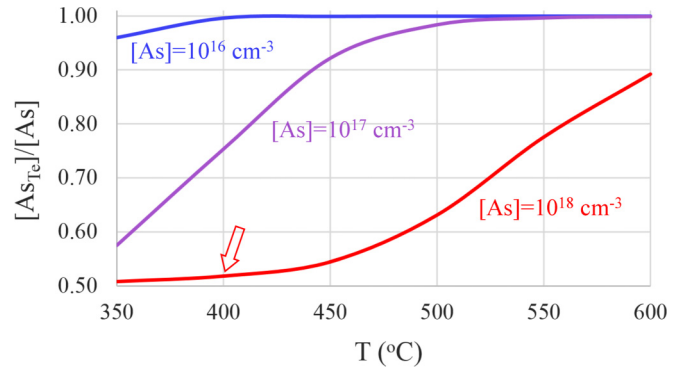

FIG. 8. Fraction of As_{Te} defects formed at stage 2 as a function of annealing temperature and total As concentration. Red arrow shows the conditions used in simulation on Fig. 6.

and the temperature of the annealing process. To study this dependence, we simulate the annealing process at temperatures ranging from 350 to 600 °C and initial arsenic concentrations from 10^{16} to 10^{18} cm^{-3}. Figure 8 shows the ratio of As_{Te}^- acceptors formed in this stage to the total amount of incorporated arsenic. Simulated trends are consistent with experimental observations that link achievable activation efficiency to the total incorporated concentration [1,3,5]. It is also worth mentioning that arsenic donor complexes not only suppress arsenic activation, but may also act as efficient recombination centers. According to our HSE calculations, (+2/+1) level of (As_iAs_i) is at 0.94 eV from valence-band maximum (VBM) and (+1/0) level is at 0.55 eV from VBM, while (As_iAs_i) complexes have ionization levels at 0.58, 0.98, and 1.21 eV. Such deep levels can cause Shockley–Read–Hall (SRH) recombination in solar cell absorber [40], which provides an additional incentive to develop processes that prevent accumulation of these complexes. To estimate the potential harm caused by SRH recombination on the deep centers formed during activation process, one needs to measure or calculate carrier capture rates (e.g., by using multiphonon transition methods [41,42]).

Stage 3: Slow increase of activation efficiency. In our simulations, we assume that removal of interstitial tellurium by-products from the system is thermodynamically favorable (from -2 to -3 eV under Te-rich and Cd-rich conditions, respectively) [12]. This means that given a choice between staying in complexes and leaving the system, tellurium by-products prefer the latter. As the compensating donor complexes dissociate letting tellurium to leave the system and releasing arsenic atoms to form new acceptors, activation efficiency increases. In fact, by increasing annealing time in our simulations, we can achieve very high activation efficiency of arsenic, eventually utilizing all the incorporated arsenic atoms as acceptors.

D. Effect of AX-center formation on slow doping decay

Our model does not predict the slow doping decay in the structures rapidly quenched after arsenic activation [1] and the dependence of doping efficiency on the cooling rate [10] reported by Nagaoka *et al.* In their work, the authors explain observed doping degradation by slow formation of

compensating AX center. We argue that this proposed mechanism becomes only possible when reaction barrier to form AX center exceeds 1 eV, while the value obtained from the first principles is much smaller. In our simulations with HSE06-calculated barrier height of 0.49 eV, we find that on cooldown to RT, reaction of AX-center formation in which As_{Te}^- traps two holes and bonds with the neighboring anion site occurs at very fast rates and completes even within a short 2-s quench. All the other reactions included in this numerical experiment become frozen during and after the cooldown.

IV. THE SCOPE AND LIMITATIONS OF OUR MODEL

Although the modern thin-film CdTe PV technology employs chlorinated CdSeTe absorbers, we limit the scope of this work to study formation of arsenic doping in a pure CdTe matrix. Here, we also perform our kinetic simulations in zero dimension, which assumes uniform concentrations at all times. The latter simplification allows omitting the details on impurity incorporation, removal of by-products, and effect of electric field. However, it also applies certain limitations that are worth mentioning. In particular, fast removal of tellurium interstitial by-products in Eq. (18) may not be the case in physical 3D situation, when tellurium association into complexes happens everywhere in the crystal bulk and segregation only occurs on the surfaces. The "effective" diffusion barrier of Te_i defects in the bulk becomes comparable to the association energy of $(As_i Te_i)^+$ complexes, which slows down Te_i removal. Our estimations using a method developed previously [43,44] suggest that at 450 °C, presence of 10^{17} cm^{-3} As_i^+ trap sites would result in up to $10^6 \times$ reduction in the effective diffusivity of Te_i^0. This means that in practical time-limited annealing steps some amount of replaced tellurium atoms may remain in donor complexes, causing incomplete activation.

The above simplifications allow us to focus on the fundamentals behind arsenic activation in CdTe and reveal the dominant activation pathway that would persist in real films. Competing diffusion-reaction processes found in real-life scenarios would definitely affect activation efficiency of arsenic in CdTe and optimal process duration; however, they will not change the dominant activation pathway revealed in this study.

V. SUMMARY AND CONCLUSIONS

In this work, we report multilevel analyses of kinetic mechanisms behind the *p*-type doping formation in CdTe by group V elements using arsenic as a model dopant. In our analysis, we use the low-level properties of defects and reactions obtained from first principles to calculate the kinetic rate constants used to simulate time-dependent changes in the concentrations of defects and free charge carrier. Our kinetic formalism relies on the detailed balance of involved reactions and includes all the thermodynamic aspects of interactions between defects and between defects and free carriers. While fully reproducing the results of equilibrium thermodynamic calculations in the limit of infinite time, our formalism also takes into account kinetic limitations imposed by the finite diffusivities of defect species and reaction barriers that slow down defect transformations.

Using this approach, we are able to go beyond the standard thermodynamic models and *simulate practical time-bound process* of group V doping activation in CdTe crystal. After thorough analysis of different mechanisms of arsenic activation, we conclude that the dominant activation pathway is via the exchange reaction where interstitial arsenic knocks out tellurium atoms from the regular lattice sites with subsequent segregation of tellurium by-products into inert stable states. We reveal that several "secondary" processes accompany this "main" activation mechanism to form kinetically stabilized transient states that compensate *p*-type doping and reduce the overall activation efficiency. The amount of compensating donor complexes formed during activation anneal depends not only on the annealing time and temperature, but also on the total amount of incorporated arsenic atoms. We also find that compensating donor complexes have deep ionization states, and might act as efficient recombination centers.

By taking into account the kinetic limitations affecting the formation of dopants as well as compensating and recombination centers, our methodology allows a significant advance in the modeling of electric properties of materials. Our approach bridges the gap between theoretical defect chemistry and analysis of practical fabrication processes. Besides practical implications for doping activation in CdTe, it could be used to study similar processes in other materials, thus advancing the overall state of the art in doping-related defect chemistry.

[1] A. Nagaoka, D. Kuciauskas, and M. A. Scarpulla, Appl. Phys. Lett. **111**, 232103 (2017).

[2] E. Colegrove, J.-H. Yang, S. P. Harvey, M. R. Young, J. M. Burst, J. N. Duenow, D. S. Albin, S.-H. Wei, and W. K. Metzger, J. Phys. D: Appl. Phys. **51**, 075102 (2018).

[3] J. M. Burst, J. N. Duenow, D. S. Albin, E. Colegrove, M. O. Reese, J. A. Aguiar, C.-S. Jiang, M. K. Patel, M. M. Al-Jassim, D. Kuciauskas, S. Swain, T. Ablekim, K. G. Lynn, and W. K. Metzger, Nat. Energy **1**, 16015 (2016).

[4] S. Farrell, T. Barnes, W. K. Metzger, J. H. Park, R. Kodama, and S. Sivananthan, J. Electron. Mater. **44**, 3202 (2015).

[5] A. Nagaoka, K.-B. Han, S. Misra, T. Wilenski, T. D. Sparks, and M. A. Scarpulla, J. Cryst. Growth **467**, 6 (2017).

[6] S. L. Rugen-Hankey, A. J. Clayton, V. Barrioz, G. Kartopu, S. J. C. Irvine, J. D. McGettrick, and D. Hammond, Sol. Energy Mater. Sol. Cells **136**, 213 (2015).

[7] G. Kartopu, L. J. Phillips, V. Barrioz, S. J. C. Irvine, S. D. Hodgson, E. Tejedor, D. Dupin, A. J. Clayton, S. L. Rugen-Hankey, and K. Durose, Prog. Photovoltaics: Res. Appl. **24**, 283 (2016).

[8] T. Ablekim, S. K. Swain, W.-J. Yin, K. Zaunbrecher, J. Burst, T. M. Barnes, D. Kuciauskas, S.-H. Wei, and K. G. Lynn, Sci. Rep. **7**, 4563 (2017).

[9] D. Kuciauskas, D. Lu, S. Grover, G. Xiong, and M. Gloeckler, Appl. Phys. Lett. **111**, 233902 (2017).

[10] A. Nagaoka, D. Kuciauskas, J. McCoy, and M. A. Scarpulla, Appl. Phys. Lett. **112**, 192101 (2018).

[11] M. A. Green, K. Emery, Y. Hishikawa, W. Warta, and E. D. Dunlop, Prog. Photovoltaics: Res. Appl. **24**, 905 (2016).

[12] J.-H. Yang, W.-J. Yin, J.-S. Park, J. Ma, and S.-H. Wei, Semicond. Sci. Technol. **31**, 083002 (2016).

[13] J.-H. Yang, W.-J. Yin, J.-S. Park, J. Burst, W. K. Metzger, T. Gessert, T. Barnes, and S.-H. Wei, J. Appl. Phys. **118**, 025102 (2015).

[14] G. Kresse and J. Furthmuller, Phys. Rev. B **54**, 11169 (1996).

[15] MedeA® version 2.19 (Materials Design Inc., Angel Fire, NM, 2011).

[16] J. P. Perdew, A. Ruzsinszky, G. I. Csonka, O. A. Vydrov, G. E. Scuseria, L. A. Constantin, X. Zhou, and K. Burke, Phys. Rev. Lett. **100**, 136406 (2008).

[17] P. E. Blöchl, Phys. Rev. B **50**, 17953 (1994).

[18] G. Kresse and D. Joubert, Phys. Rev. B **59**, 1758 (1999).

[19] J. Heyd, G. E. Scuseria, and M. Ernzerhof, J. Chem. Phys. **118**, 8207 (2006).

[20] S.-H. Wei and S. B. Zhang, Phys. Rev. B **66**, 155211 (2002).

[21] D. Krasikov, A. Knizhnik, B. Potapkin, S. Selezneva, and T. Sommerer, Thin Solid Films **535**, 322 (2013).

[22] J. Ma and S.-H. Wei, Phys. Rev. Lett. **110**, 235901 (2013).

[23] M.-H. Du, H. Takenaka, and D. J. Singh, J. Appl. Phys. **104**, 093521 (2008).

[24] J. Ma, J. Yang, S.-H. Wei, and J. L. F. Da Silva, Phys. Rev. B **90**, 155208 (2014).

[25] Y. Yin, G. Chen, H. Ye, X. Duan, Y. Zhu, and Y. Wu, Europhys. Lett. **114**, 36001 (2016).

[26] F. A. Kröger, *The Chemistry of Imperfect Crystals* (North-Holland, Amsterdam, 1964).

[27] P. Atkins and J. de Paula, *Atkins' Physical Chemistry*, 8th ed. (W. H. Freeman, New York, 2006).

[28] X. Zhang, B. Grabowski, T. Hickel, and J. Neugebauer, Comput. Mater. Sci. **148**, 249 (2018).

[29] D. N. Krasikov, A. V. Scherbinin, A. A. Knizhnik, A. N. Vasiliev, B. V. Potapkin, and T. J. Sommerer, J. Appl. Phys. **119**, 085706 (2016).

[30] D. Krasikov and I. Sankin, J. Mater. Chem. A **5**, 3503 (2017).

[31] C. Freysoldt, B. Grabowski, T. Hickel, J. Neugebauer, G. Kresse, A. Janotti, and C. G. Van de Walle, Rev. Mod. Phys. **86**, 253 (2014).

[32] S. K. Estreicher, M. Sanati, D. West, and F. Ruymgaart, Phys. Rev. B, **70**, 125209 (2004).

[33] J. Ma, S.-H. Wei, T. A. Gessert, and K. K. Chin, Phys. Rev. B **83**, 245207 (2011).

[34] V. Kuzovkov and E. Kotomin, Rep. Prog. Phys. **51**, 1479 (1998).

[35] P. Hänggi, P. Talkner and M. Borkovec, Rev. Mod. Phys. **62**, 251 (1990).

[36] J.-H. Yang, J.-S. Park, J. Kang, and S.-H. Wei, Phys. Rev. B **91**, 075202 (2015).

[37] K. Wolf and W. M. Bartczak, in *Proceedings of SPIE 4412, International Conference on Solid State Crystals 2000: Growth, Characterization, and Applications of Single Crystals*, Vol. 4412 (SPIE, 2001), p. 137.

[38] D. Krasikov, A. Knizhnik, B. Potapkin, and T. Sommerer, MRS Online Proceedings Library **1638**, 1 (2014).

[39] R. Grill and A. Zappetini, Prog. Cryst. Growth Charact. Mater. **48/49**, 209 (2004).

[40] Z. Cheng, A. E. Delahoy, Z. Su, and K. K. Chin, Thin Solid Films **558**, 391 (2014).

[41] L. Shi, K. Xu, and L.-W. Wang, Phys. Rev. B **91**, 205315 (2015).

[42] A. Alkauskas, Q. Yan, and C. G. Van de Walle, Phys. Rev. B **90**, 075202 (2014).

[43] R. A. Oriani, Acta Metall. **18**, 147 (1970).

[44] Y. Sakamoto, Trans. Jpn. Inst. Metals **25**, 244 (1984).